

Smectic-*C* – smectic-*I* critical point in a liquid crystal mixture: Static and dynamic thermal behavior

Haruhiko Yao,* Tom Chan,[†] and Carl W. Garland

*School of Science and Center for Material Science and Engineering, Massachusetts Institute of Technology,
Cambridge, Massachusetts 02139*

(Received 8 December 1994)

The theoretically predicted smectic-*C* (Sm-*C*)–smectic-*I* (Sm-*I*, a tilted hexatic phase) critical point has been discovered in a racemic mixture of methylbutyl phenyl octylbiphenyl-carboxylate (8SI) and the octyloxybiphenyl analog (8OSI). High-resolution ac calorimetry and nonadiabatic scanning calorimetry show an evolution from a first-order Sm-*C*–Sm-*I* transition in 8SI to continuous supercritical behavior in 8OSI (no thermodynamic transition). The critical composition is $X_c \simeq 75$, where X is the weight percent 8OSI. The static critical heat capacity $C_p(T, X=75)$ is characterized by a critical exponent $x = 1.06 \pm 0.08$ that corresponds to the exponent γ due to the path of approach to the critical point. This is a mean-field value of γ rather than the value associated with the new universality class that includes Sm-*C*–Sm-*I*, Sm-*C**–Sm-*C**, and Sm-*A*_d–Sm-*A*₂ (partial bilayer–bilayer smectic) critical points. It is proposed that mean-field behavior is observed due to long bare correlation lengths (Ginzburg criterion). Note that $C_p(T, X)$ measured along the path $X = X_c$ is effectively a susceptibility, like C_p for a pure fluid near its liquid-gas critical point. Data obtained close to T_c show a systematic frequency dependence, and these $C_p(T, \omega)$ data are discussed in terms of critical slowing down and dynamic scaling behavior.

PACS number(s): 64.70.Md, 64.60.Fr, 65.20.+w

I. INTRODUCTION

Hexatic liquid crystal phases, which exhibit long-range bond-orientational (BO) order but only short-range in-plane positional order, are not yet well understood. In particular, the universality characteristics of the smectic-hexatic transition are still unresolved. Studies of smectic-*A* (Sm-*A*)–hexatic-*B* (Hex-*B*) transitions have included high-resolution x-ray diffraction [1] and an extensive series of heat-capacity measurements on bulk and thin film samples [2–7]. Almost all Sm-*A*–Hex-*B* transitions appear to be second order, although in some cases the C_p peak is rounded over an interval of 50–200 mK about the transition temperature. The heat-capacity critical exponent for a wide variety of bulk compounds and binary mixtures is in the range 0.50–0.65, which differs markedly from the three-dimensional (3D) XY value $\alpha = -0.007$ that might be expected since the BO order parameter $\Psi = |\Psi| \exp(i6\psi)$ has XY symmetry. Theoretical models have proposed an important role for coupling between the hexatic order parameter and herringbone order $\Phi = |\Phi| \exp(i2\varphi)$ [8], crystalline order [9], or layer displacement u [10]. The applicability of these models to the bulk Sm-*A*–Hex-*B* transitions is unclear, but a recent 2D simulation of a coupled XY model with hexatic and

herringbone order [11] yields a new type of phase transition that appears to be compatible with the critical exponent $\alpha = 0.30 \pm 0.05$ observed for two-layer liquid crystal films [7].

Tilted hexatic phases can also occur on cooling some tilted smectic-*C* (Sm-*C*) materials. In this case, there are two hexatic structures where long-range BO order is combined with long-range molecular tilt of the director with respect to the layer normal—Sm-*I* (where the tilt is towards a nearest neighbor) and Sm-*F* (where the tilt direction is between two nearest neighbors). The presence of BO order in Sm-*I* (Sm-*F*) does not, however, change the point group symmetry from that of Sm-*C*. As a result, the situation is qualitatively analogous to that for a liquid-vapor transition in a simple fluid. There can be either a first-order phase transition between Sm-*C* and Sm-*I* (Sm-*F*) or no thermodynamic phase transition at all, but a supercritical evolution of both BO order and tilt in a single phase that is conventionally called “Sm-*C*” at high temperatures and “Sm-*I* (Sm-*F*)” at lower temperatures [12,13]. Thus, in some suitable phase diagram there must exist an isolated critical point. This Sm-*C*–Sm-*I* (Sm-*F*) critical point is predicted to belong to the same universality class as Sm-*A*–Sm-*A* and electric-field-induced chiral Sm-*C**–Sm-*C** critical points [13], although mean-field behavior cannot be ruled out if the data lie outside the Ginzburg critical regime.

The presence of a coupling between the molecular tilt and the bond-orientation order means that an external magnetic field can produce a single-domain tilted hexatic sample. This is crucial for high-resolution x-ray investigations of the nature of Sm-*I* and Sm-*F* phases. Detailed

*Present address: Department of Physics, Tokyo Institute of Technology, O-okayama, Meguro-ku, Tokyo 152, Japan.

[†]Present address: Microcal Software, Roundhouse Plaza, Northampton, MA 01060.

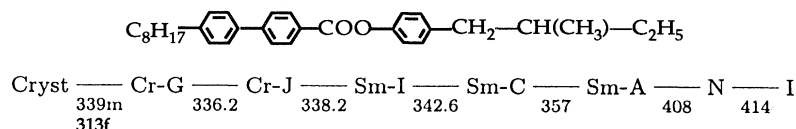
x-ray [14] and heat-capacity [15] studies have been made of 8OSI [racemic 4-(2'-methylbutyl) phenyl 4'-(octyloxy)-biphenyl-4-carboxylate], which exhibits a supercritical Sm-C–Sm-I evolution. The behavior of the sixfold hexatic order parameter C_6 and its higher harmonics C_{6n} in bulk films at temperatures below the “transition” region agrees very well with a multicritical scaling relation developed for a system with basic XY symmetry [9]. The temperature dependence in the transition region of C_6 and the excess heat capacity ΔC_p associated with the growth of hexatic order have been analyzed in terms of a phenomenological parametric equation of state [15]. However, the appropriateness of this model and the interpretation of the effective C_p critical exponent 0.47 and the C_6 order parameter exponent 0.077 are not clear. X-ray [16] and heat-capacity [17] studies have also been made of TB5A, TB6A, and TB7A [pentyl, hexyl, and heptyl homologs of terephthal-bis-(4*n*)-alkylaniline], which exhibit Sm-C–Sm-F transitions. In all three cases, this transition is strongly first order, although there are appreciable pretransitional effects both above and below the transition temperature.

The goal of the present investigation is to identify the location of a Sm-C–Sm-I critical point and characterize the critical behavior associated with heat capacity at that point. It is clear that a Sm-C–Sm-F critical point will not be realized in mixtures of TB*n*A homologs since the pure compounds all exhibit first-order behavior. Howev-

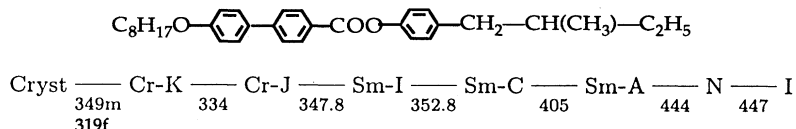
er, the prospect of a Sm-C–Sm-I critical point in mixtures of 8OSI and 8SI (the octylbiphenyl analog of 8OSI) was very promising. Light scattering studies [18] have shown that the coupling between BO order and tilt is smaller by a factor of $\sim 10^2$ in 8SI than that in 8OSI. Thus the effective field due to the tilt that induces finite BO order in the Sm-C phase is small in 8SI and one would expect a first-order Sm-C–Sm-I transition. Indeed, first-order Sm-C–Sm-I transitions have been observed in thin 8SI films [18]. Furthermore, structure and miscibility studies [19] show that mixtures of 8SI and 8OSI have Sm-C, Sm-I, and plastic crystal Cr-J phases that are miscible across the entire composition range. The experimental results given in Sec. II show that there is a Sm-C–Sm-I critical point at a concentration $X_c \simeq 75$, where X is the weight percent 8OSI. Interesting static and dynamic critical behavior was observed near T_c for this mixture. The static critical behavior associated with $C_p(X_c, T)$ and the critical dynamics at very low frequencies are analyzed and discussed in Sec. III. A brief summary is provided in Sec. IV.

II. EXPERIMENTAL METHOD AND RESULTS

The structural formulas and phase transition sequences on cooling for racemic 8SI ($M=456.7 \text{ g mol}^{-1}$) and 8OSI ($M=472.7 \text{ g mol}^{-1}$) are for 8SI (also denoted $\pm 2M4P8BC$) [20]



and for 8OSI (also denoted $\pm 2M4P80BC$) [15,20]



All the transition temperature values are in kelvin; both the melting (*m*) and freezing (*f*) points are given for the rigid crystal denoted as Cryst. The symbols Cr-G, Cr-J, and Cr-K represent plastic crystal phases; Sm-I is the tilted hexatic smectic-I phase; Sm-A and Sm-C denote smectic-A and smectic-C phases; N is the nematic phase and I is the isotropic phase. Note that the width of the Sm-C phase is 14.4 K for 8SI and 52.2 K for 8OSI. This suggests a correlation between the Sm-C width and the character of the Sm-C–Sm-I transition. The smectic free energy density contains the term $-H\Psi = -(h_6 + h_{12})|\theta|^6\Psi$, where $|\theta|$ is the tilt angle and h_6 (h_{12}) is the coefficient for a coupling term of sixfold (twelfold) symmetry [18]. Thus the effective tilt field $H \sim |\theta|^6$ increases rapidly with the value of the tilt angle at the Sm-C–Sm-I transition temperature even if the coupling coefficients do not vary. When the tilt is well developed (almost saturated as in 8OSI [18,20]), the value of H will be large and

BO order will develop as a supercritical evolution. When the tilt is less developed (as in 8SI [19,21]) one would expect a smaller value of H , which leaves the Sm-C–Sm-I transition first order.

A partial phase diagram for 8SI plus 8OSI mixtures is given in Fig. 1. The transition lines have been taken from Ref. [19] and the Sm-C–Sm-I transition temperatures obtained in the present calorimetric study are shown as open circles. Samples of 8SI, 8OSI, and mixtures with $X=50, 75, 85$ w. % 8OSI were studied in detail. Preliminary measurements were also made on a mixture with $X=60$. Since the $C_p(T)$ behavior for this sample was qualitatively very similar to that for $X=50$, no high density data were taken and no C_p data are reported for this $X=60$ sample.

A small mass of each liquid crystal sample, typically 40 mg, was sealed (under an atmosphere of dry nitrogen gas) into a silver cell along with a helical coil of gold wire to

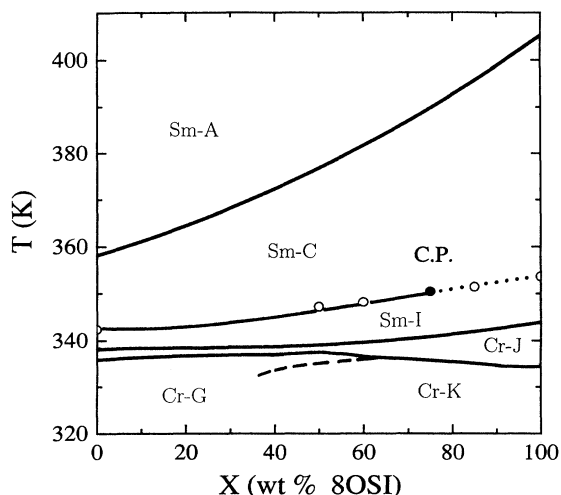


FIG. 1. Partial phase diagram of 8SI plus 8OSI mixtures; X is the weight percent 8OSI. The lines are taken from Ref [19] and the open circles represent Sm-C-Sm-I transition temperatures obtained from the present C_p measurements. Since our data indicate that the Sm-C-Sm-I critical point (C.P.) lies at $X \approx 75$, the dotted line for $X > 75$ merely represents the locus of extrema in the thermodynamic response functions (maximum C_p in the present case). No thermodynamic transition occurs in this supercritical region.

enhance the thermal conductivity and eliminate any internal temperature gradients. Some of the data were obtained on the high-resolution ac calorimeter used previously at MIT and described elsewhere [22]. Other data were taken on a new and improved high-resolution calorimeter that can be operated in the standard ac mode and also in relaxation modes. This instrument is based on the design described by Ema *et al.* [23] and its operation will be briefly described below. In both modes, the bath temperature is scanned slowly. In the ac mode, scan rates of 15–100 mK/h were used near T_c for the near-critical $X=75$ mixture and somewhat faster rates (100–200 mK/h) were used near $C_p(\max)$ for 8OSI and the other mixtures. In the linear-ramp relaxation mode (nonadiabatic scanning), a scan rate of 1 K/h was used.

A. Automated high-resolution calorimeter

Heat-capacity measurements were made with a computerized calorimeter capable of fully automated operation in either ac or relaxation modes. The sample (in a sealed silver cell) is thermally linked to a temperature-controlled thermal bath partly by support wires and partly by air, which acts as an exchange gas. This thermal link can be represented by a thermal resistance R , which is the reciprocal of the thermal conductance Λ .

In the ac mode, an oscillating heat input $P_{ac} \exp(i\omega t)$ is supplied to the sample by a thin resistive heater. The frequency ω of the power input is chosen so that $\omega\tau_{int} \ll 1$, where τ_{int} is the relaxation time for thermal diffusion in the sample cell. Thus the temperature oscillations induced in the sample are slow enough that temperature gradients in the sample are negligibly small. In this case,

the complex amplitude T_{ac} of the sample temperature oscillation is given by

$$T_{ac} = \frac{P_{ac}}{R^{-1} + i\omega C}, \quad (1)$$

where C represents the heat capacity of the sample cell. This quantity can in general be complex and frequency dependent:

$$C^*(\omega) = C'(\omega) - iC''(\omega), \quad (2)$$

with $C'(\omega)$ and $C''(\omega)$ being the real and the imaginary parts, respectively. Combining Eqs. (1) and (2), one finds [23]

$$|T_{ac}| = \frac{|P_{ac}|}{\omega C'(\omega)} \left\{ 1 + \left[\frac{1}{\omega R C'(\omega)} + \frac{C''(\omega)}{C'(\omega)} \right]^2 \right\}^{-1/2}, \quad (3)$$

$$\Phi = -\frac{\pi}{2} + \arctan \left[\frac{1}{\omega R C'(\omega)} + \frac{C''(\omega)}{C'(\omega)} \right] \quad (4)$$

for the amplitude of the ac temperature oscillation and the phase shift Φ of T_{ac} with respect to P_{ac} . Solving these equations for $C'(\omega)$ and $C''(\omega)$ yields

$$C'(\omega) = -\frac{|P_{ac}|}{\omega |T_{ac}|} \sin \Phi = \frac{|P_{ac}|}{\omega |T_{ac}|} \cos \phi, \quad (5)$$

$$C''(\omega) = \frac{|P_{ac}|}{\omega |T_{ac}|} \cos \Phi - \frac{1}{\omega R} = \frac{|P_{ac}|}{\omega |T_{ac}|} \sin \phi - \frac{1}{\omega R}, \quad (6)$$

where $\Phi \equiv \phi - \pi/2$. In many cases, the heat capacity is a purely real frequency-independent quantity: $C'(\omega) = C(0) = C$ and $C''(\omega) = 0$. For the usual mode of operation of an ac calorimeter, ω is chosen so that $\omega RC \gg 1$. In this limit, the heat capacity is given by the simple expression $C = |P_{ac}| / \omega |T_{ac}|$. Note that for our calorimeter at the standard operating frequency $\omega_0 = 0.196$ (32-s period for T_{ac}), ϕ is typically 0.1–0.2 rad and $\cos \phi \approx 0.98 - 1$. The use of Eqs. (3)–(6) allows us to analyze data for samples with a complex frequency-dependent heat capacity using frequencies lower than those required by the so-called adiabatic condition $\omega RC \gg 1$. This is important since one must also satisfy the condition $\omega\tau_{int} \ll 1$ in order to avoid temperature gradients inside the sample near T_c , and this sets an upper bound on ω for any given cell design. The value of R needed in Eq. (6) can be determined accurately from relaxation measurements as described below.

In the relaxation mode, conventional operation uses a dc power supplied to the cell that is a step function. For a heating run, P is switched from 0 at time $t=0$ to a constant value P_0 , whereas the power is switched from P_0 to 0 for a cooling run. It follows that the cell temperature $T(t)$ relaxes exponentially [23]

$$T(t) = T_B + \Delta T_\infty [1 - \exp(-t/\tau_{ext})] \quad (7a)$$

for the heating regime and

$$T(t) = T_B + \Delta T_\infty \exp(-t/\tau_{ext}) \quad (7b)$$

for the cooling regime, where T_B is the constant bath

temperature and $\Delta T_\infty = RP_0$. The quantity $\tau_{\text{ext}} = RC$ is the "external" time constant for heat flow from the sample to the bath.

In the present experiment, relaxation measurements were made with the heater power linearly ramped. For a heating run, $P=0$ for $t < 0$, $P=\dot{P}t$ for $0 \leq t \leq t_1$, and $P=P_0=\dot{P}t_1$ for $t > t_1$. The initial ($t \leq 0$) sample temperature is T_B and the plateau sample temperature is $T(\infty) = T_B + RP_0$ for $t \gg t_1$. For a cooling run, the power profile is reversed: $P=P_0$ for $t < 0$, $P=P_0 + \dot{P}t$ with \dot{P} negative for $0 \leq t \leq t_1$, and $P=0$ for $t > t_1$. In this case the sample temperature is initially $T(\infty)$ and has the final value T_B . The variation of the cell temperature over the time regime $0 \leq t \leq t_1$ is

$$T(t) = T_B + R\dot{P}(t - \tau_{\text{ext}}) + t_{\text{ext}}R\dot{P} \exp(-t/\tau_{\text{ext}}) \quad (8a)$$

for the heating regime with \dot{P} positive and

$$T(t) = T(\infty) + R\dot{P}(t - \tau_{\text{ext}}) + \tau_{\text{ext}}R\dot{P} \exp(-t/\tau_{\text{ext}}) \quad (8b)$$

for the cooling regime with \dot{P} negative. The thermal resistance is given by

$$R = (T_\infty - T_B)/P_0 \quad (9)$$

and the heat capacity for heating or cooling runs is

$$C(T) = \frac{dH}{dT} = \frac{P - (T - T_B)/R}{dT/dt}, \quad (10)$$

where P is the power at time t' corresponding to sample temperature T lying in the interval T_B to $T(\infty)$ and dT/dt is obtained by fitting $T(t)$ data over a short time interval centered at t' . The advantages of this new ramp relaxation method, which could best be called nonadiabatic scanning calorimetry, over the use of a power step function are (a) much better control of the bath temperature T_B at a constant value since step increases or decreases in P cause large transient disturbances in T_B and (b) optimal behavior of dT/dt since T varies almost linearly with t (except for $t > t_1$ and a brief period just after $t=0$ and of course regions where the enthalpy H is an unusually rapid varying function of T due to first-order phase conversion).

B. Heat capacity data

For much of the present work, the heat capacity is a real, frequency-independent quantity that was measured only at our standard ac frequency $\omega_0 = 0.196$ under conditions where $\omega_0 RC \gg 1$. In this case, Eqs. (3) and (4) reduce to the familiar forms [22]

$$C^2 = \frac{|P_{\text{ac}}|^2}{\omega^2 |T_{\text{ac}}|^2} - \frac{1}{\omega^2 R^2} \simeq \frac{|P_{\text{ac}}|^2}{\omega^2 |T_{\text{ac}}|^2}, \quad (11)$$

$$\tan(\Phi + \pi/2) = \tan\phi = 1/\omega RC \quad (12a)$$

or

$$\tan\Phi = -\omega RC. \quad (12b)$$

However, for near-critical and supercritical samples, frequency-dependent complex heat capacities were ob-

served near the maximum in the Sm-C-Sm-I excess heat-capacity peak. In this case, data were taken at four frequencies ($2\omega_0$, ω_0 , $\omega_0/3$, and $\omega_0/9$). Since C becomes complex near its maximum and $\omega RC_p \gg 1$ does not hold at the lower frequencies, Eqs. (5) and (6) must be used along with R values obtained from the relaxation method to determine $C'(\omega)$ and $C''(\omega)$. Details of the C_p dispersion, i.e., frequency dependence of C_p , are given for the near-critical sample with $X=75$.

Once the heat capacity of the filled cell has been determined, the specific heat capacity of the sample is given by

$$\text{Im}C_p(\omega) = C''_{\text{filled}}(\omega)/m, \quad (13)$$

$$\text{Re}C_p(\omega) = [C'_{\text{filled}}(\omega) - C_{\text{empty}}]/m, \quad (14a)$$

$$C_p(\omega) \equiv |C_p^*(\omega)| = \{[\text{Re}C_p(\omega)]^2 + [\text{Im}C_p(\omega)]^2\}^{1/2}, \quad (14b)$$

where $C'_{\text{filled}}(\omega)$ and $C''_{\text{filled}}(\omega)$ are the real and the imaginary heat capacities of the filled cell, C_{empty} is the heat capacity of the empty cell (a purely real quantity determined at ω_0), and m is the mass of liquid crystal sample in grams. The quantity $C_p(\omega)$ is taken to be $|C_p^*(\omega)|$ rather than $\text{Re}C_p(\omega)$ since $|C_p^*(\omega)|$ is closer to the static value $C_p(0)$ when critical relaxation exists.

The heat capacity of pure 8SI is shown in Fig. 2 over a 13° temperature range that includes Sm-C-Sm-I, Sm-I-Cr-J, and Cr-J-Cr-G transitions at 342.38, 338.35, and 336.70 K, respectively. All three transitions are first order and the thermal anomalies at the Sm-I-Cr-J and Cr-J-Cr-G transitions are quite small, as expected from

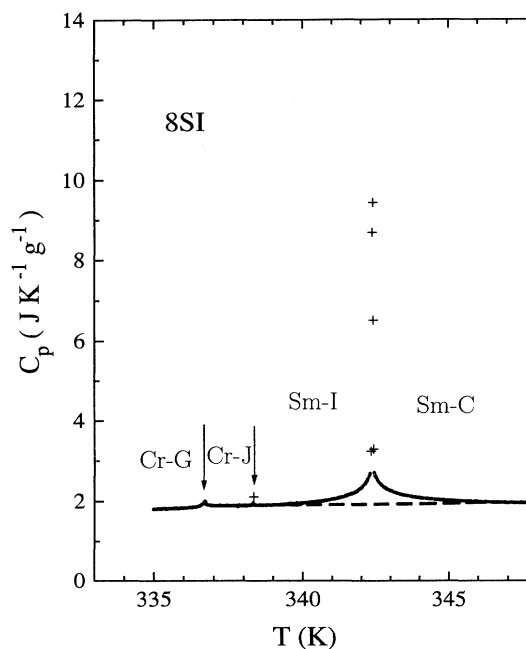


FIG. 2. Heat capacity of 8SI. Data were obtained at $\omega_0 = 0.196$ and represent static specific heats $C_p(\omega=0)$. The points marked by a plus symbol are not true heat capacities, but indicate apparent C_p values obtained in a two-phase coexistence region. Arrows indicate the very small anomalies at the Sm-I-Cr-J and Cr-J-Cr-G transitions.

differential scanning calorimetry runs on 8SI [19] and ac calorimetry on the Sm-I-Cr-J transition in 8OSI [15]. The data in Fig. 2 were obtained on a slow cooling run and appreciable hysteresis may occur for the Sm-I-Cr-J and Cr-J-Cr-G transitions since the kinetics of these transitions is reported to be extremely slow [19]. Although there are distinct pretransitional C_p wings, the Sm-C-Sm-I transition is quite strongly first order with five data points observed in a 125-mK-wide coexistence region. The presence of two-phase coexistence is signaled by an abrupt increase in the phase angle ϕ and by anomalously large apparent C_p values [23]. The dashed line in Fig. 2 represents the background heat capacity $C_{p,B}$ that would be expected in the absence of the Sm-C-Sm-I transition.

Heat-capacity data obtained at ω_0 for pure 8OSI and three mixtures of 8SI plus 8OSI are shown in Fig. 3. The quantity displayed here is the excess heat capacity $\Delta C_p = C_p - C_{p,B}$ that is obtained by subtracting a linear (nearly constant) background heat capacity $C_{p,B}$. For the 50% sample, the Sm-C-Sm-I transition is first order with six anomalous points obtained in a 100-mK-wide coexistence region centered at 347.20 K on cooling. This was confirmed by a very slow cooling run at $\omega_0/3$, which exhibited 12 anomalous points over the same coexistence region. Preliminary data (not shown) on a 60% sample indicated a first-order coexistence region of about 70 mK. For the three samples with 8OSI weight percent $X \geq 75$, there is no indication of two-phase coexistence. In these samples, the C_p peaks are smoothly rounded and frequen-

cy dependent near the maximum, as will be described in detail for the 75% sample. The ΔC_p data for pure 8OSI given in Fig. 3, including the small Sm-I-Cr-J feature observable at 348.45 K, are in good agreement with those reported previously [15]. The heat-capacity data shown in Fig. 3 were all obtained on slow cooling scans with typical scan rates of ~ 100 mK/h. The results were reproducible on heating runs and on repeat cooling runs with little or no drift in the position T_{\max} of the ΔC_p maxima. No change in the value of T_{\max} was observed over 10 days of $X=50$ and 75; the T_{\max} drift was -5 mK/day for $X=85$ and -14 mK/day for $X=100$.

In view of the magnitude and sharpness of the ΔC_p peak for the 75% sample, we believe that the critical concentration is close to $X=75$. The heat capacity of this near-critical sample is shown over a wide temperature range in Fig. 4, which displays the large $C_p(\omega_0)$ peak associated with the Sm-C-Sm-I critical region and the very small Sm-I-Cr-J feature at 344.85 K. The background value $C_{p,B}$, shown by the dashed line is given by $C_{p,B} = 2.34 + 0.0062(T - T_c)$ in $\text{J K}^{-1} \text{g}^{-1}$ units, where the critical temperature $T_c = 350.393$ K is taken to correspond to the position of the C_p maximum. A plot of $\Delta C_p(\omega) = C_p(\omega) - C_{p,B}$ for temperatures close to T_c is given in Fig. 5 for $\omega = \omega_0, \omega_0/3$, and $\omega_0/9$. Also shown in this figure is the ΔC_p variation determined from a slow nonadiabatic scanning (ramp relaxation) run with sample temperature variations of 18 mK/min near T_c . This value can be compared with the sample's oscillating temperature dependence \dot{T} during ac measurements at $\omega_0/9$. In that case, the linear scanning rate for the average sam-

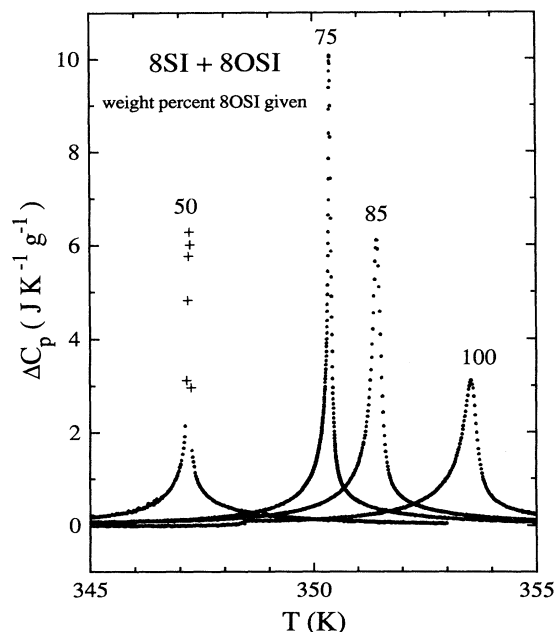


FIG. 3. Excess heat capacity ΔC_p associated with the Sm-C-Sm-I transition in 8SI plus 8OSI mixtures with weight percent 8OSI concentration $X=50, 75, 85$, and 100 (pure 8OSI). The data shown here were all obtained at $\omega_0=0.196$ and represent $C_p(\omega_0)$ defined by Eq. (14b). As in Fig. 2, points denoted by a plus sign represent artificial values obtained in a two-phase coexistence region.

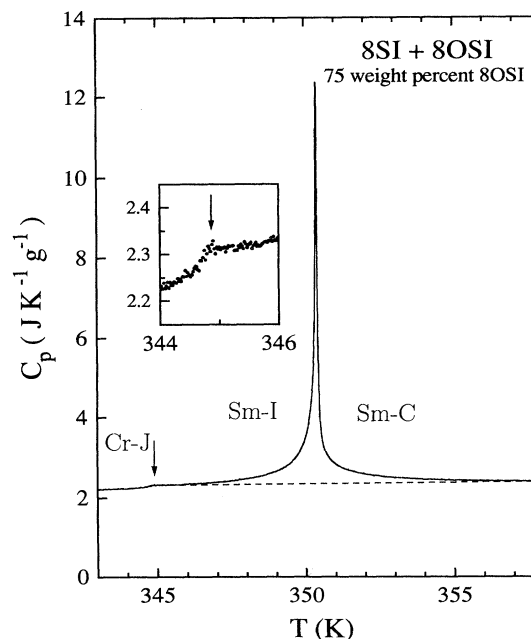


FIG. 4. Heat capacity $C_p(\omega_0)$ for the near-critical 8SI plus 8OSI mixture with 75 w. % 8OSI. The inset gives an expanded view of the Sm-I-Cr-J transition region. The dashed line representing the background heat capacity $C_{p,B}$ has the empirical form $2.34 + 0.0062(T - T_c)$ in $\text{J K}^{-1} \text{g}^{-1}$.

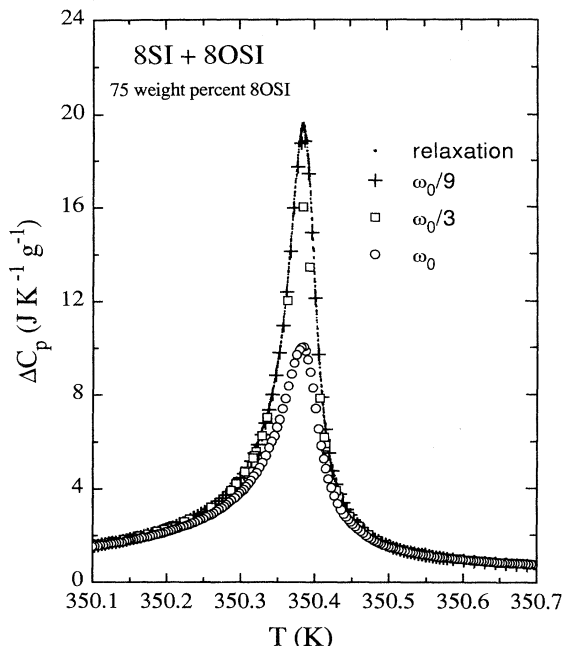


FIG. 5. Frequency-dependent magnitude $C_p(\omega) = |C_p^*(\omega)|$ of the complex heat capacity near T_c for the near-critical mixture with 75 w. % 8OSI. $\Delta C_p = C_p(\omega) - C_{p,B}$ where $C_p(\omega)$ is defined by Eq. (14b); see the text for details about the nonadiabatic scanning (relaxation) data.

ple temperature was -0.17 mK/min and the oscillatory variation $\dot{T} = \omega T_{ac} \cos \omega t$ had a maximum value ωT_{ac} of about 12 mK/min near T_c . Thus the “effective frequency” of the non-adiabatic scanning run is quite comparable to $\omega_0/9$, which is consistent with the agreement between data obtained in those two runs. Furthermore, the non-adiabatic scanning run shows that there is no hidden latent heat associated with a first-order Sm-C–Sm-I transition for the 75% mixture.

A frequency dependence for $\text{Re}C_p(\omega)$ and nonzero values for $\text{Im}C_p(\omega)$ are observed over the range -0.35 K $< \Delta T < +0.25$ K, where $\Delta T = T - T_c$. The $\text{Im}C_p(\omega)$ data near T_c in the near-critical 75% mixture are shown in Fig. 6. As expected, $\text{Im}C_p(\omega)$ is quite small and limited to temperatures very close to T_c for the low frequency $\omega_0/9$, but becomes significant over a range of about $T_c \pm 0.3$ K at ω_0 and $2\omega_0$. For the quantity $C_p(\omega) = |C_p^*(\omega)|$, we have observed excellent agreement among $C_p(\omega)$ values for frequencies in the range $\omega_0 - \omega_0/9$ over the ranges $+0.12$ K $< \Delta T < +0.67$ K and -0.79 K $< \Delta T < -0.023$ K (see Fig. 5). Thus $C_p(\omega_0)$ corresponds to the static thermodynamic limiting value $C_p(0)$ except very close to T_c . The same conclusion holds for supercritical samples with $X=85$ and 100 (pure 8OSI), where frequency-dependent C_p values were observed near the maximum in $C_p(T)$, but not in the wings of the C_p peak.

III. ANALYSIS AND DISCUSSION

This section is concerned with both the critical behavior of the static heat capacity for the near-critical

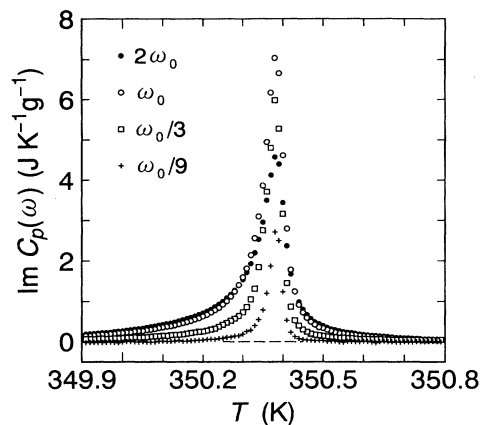


FIG. 6. Temperature dependence of $\text{Im}C_p(\omega)$ for the near-critical mixture with 75 w. % 8OSI. This quantity was calculated from Eqs. (6) and (13). Data are included for $2\omega_0$, a frequency that was not included in the display given in Fig. 5.

75% mixture and the dynamical behavior observed near T_c for that sample.

A. Static critical behavior

The heat capacity of the 75% mixture has been analyzed over the range from 346.4 to 354.4 K, which corresponds to a maximum reduced temperature $\tau = |T - T_c|/T_c$ of 1.14×10^{-2} . Data obtained at ω_0 were used far from T_c , but only data obtained at $\omega_0/9$ were used over the ranges $T - T_c = +0.022$ to $+0.2$ K and -0.0035 to -0.3 K. To avoid the region of finite-frequency rounding even at $\omega_0/9$, we have excluded data from 350.359 to 350.416 K. Thus the minimum τ values are 6.3×10^{-5} above T_c and 1.0×10^{-4} below T_c .

Fits were based on the power-law form

$$C_p = A^\pm \tau^{-x} (1 + D^\pm \tau^{\Delta_1} + \dots) + B + E(T - T_c) \quad (15)$$

as the starting point. Due to the path of approach to the Sm-C–Sm-I critical point, the exponent x is not the usual α , as described later. We will also allow the possibility that Δ_1 differs from its usual value of 0.5. For convenience, Eq. (15) will be rewritten as

$$C_p = A_1^\pm \tau^{-x} + A_2^\pm \tau^{-y} + A_3^\pm \tau^{-y'} + B + E(T - T_c), \quad (16a)$$

where y is an effective exponent representing $x - \Delta_1$, y' is a higher-order correction exponent, and $A_2^\pm = A^\pm D^\pm$. The linear term with slope E arises from the regular (non-critical) contributions to C_p , whereas the constant $B = B_r + B_c$ represents a combination of both regular and critical contributions. A variety of fits over three ranges are summarized in Table I. A simple power-law form (i.e., $A_2^\pm = 0$ and $A_3^\pm = 0$) was used for fits 1, 3, and 5. This type of fit is very poor for range C, and physically unreasonable values were obtained in all three fits for the slope E compared with the value $E = 0.0062$ J K $^{-2}$ g $^{-1}$ shown in Fig. 4. In any case, these three fits indicate that the critical exponent x must be large (close to 1) and strongly suggest that correction terms play a very important role. Several fits over range C ($\tau_{\text{max}} = 1.14 \times 10^{-2}$)

TABLE I. Least-squares values of the adjustable parameters for fitting C_p data of the 75% 8OSI sample with Eqs. (16a) and (16b). Quantities held fixed during a fit are enclosed in square brackets. Range A (96 points) has $\tau_{\max}=8\times 10^{-4}$, range B (171 points) has $\tau_{\max}=2.3\times 10^{-3}$, and range C (588 points) has $\tau_{\max}=1.14\times 10^{-2}$, τ_{\min} values are 6.3×10^{-3} and -1.0×10^{-4} . The units of A_1^\pm , A_2^\pm , and B are $\text{J K}^{-1} \text{g}^{-1}$; the units of E are $\text{J K}^{-2} \text{g}^{-1}$. $\Delta B=B^+-B^-$. $A_3^\pm=0$ unless otherwise noted. The estimated standard deviation for C_p data points is $\sigma=0.003C_p$.

Fit	Range	T_c (K)	B^+	ΔB	x	y	$10^4 A_1^+$	A_1^-/A_1^+	A_2^+	A_2^-/A_2^+	E	χ_v^2
1	A	350.392	2.485	[0]	0.935		7.90	2.49	[0]	[1]	0.106	2.1
2	A	350.391	2.340	-0.374	0.942		7.89	2.24	[0]	[1]	0.663	2.0
3	B	350.392	2.462	[0]	0.930		8.25	2.51	[0]	[1]	0.163	2.7
4	B	350.392	2.455	-0.013	0.930		8.33	2.49	[0]	[1]	0.172	2.7
5	C	350.389	2.316	[0]	0.876		15.26	2.11	[0]	[1]	0.034	14.2
6	C	350.397	2.216	[0]	1.010	$x-0.5$	1.87	5.54	0.018	0.587	0.014	4.0
7	C	350.394	1.58	[0]	0.979	0.129	4.27	3.14	0.45	0.86	0.0075	1.7
8	C	350.393	2.455	0.307	0.871		13.78	2.68	[0]	[1]	-0.0165	5.3
9	C	350.394	2.228	0.200	1.121	0.501	0.73	4.06	0.020	1.51	0.0046	2.1
10	C	350.394	2.254	0.206	1.075	[0.5]	1.24	3.70	0.018	1.50	0.0028	2.0
11	C	350.394	1.948	0.200	[1]	0.211	3.38	3.19	0.176	1.13	0.0021	1.5
12	C	350.394	2.299	0.200	[1]	[0.5]	2.77	3.61	0.014	1.27	-0.0016	2.5
13 ^a	C	350.392	2.655	0.605	[1]	[0.5]	3.98	2.23	0.0022	10.5	0.0008	1.0
14 ^a	C	350.391	2.501	0.350	1.057	$x-0.5$	2.10	2.17	0.0050	3.97	-0.0446	1.15
15 ^a	C	350.392	2.20	0.12	1.12	0.49	0.9 ± 1.7	2.8	0.018	2.13	-0.0508	1.3

^aFor these fits $A_3^\pm \neq 0$; see the text.

were carried out with the confluent singularity $A_2^\pm \tau^{-y}$ taken into account. Fit 6 is based on $\Delta_1=0.5$ and therefore $y=x-0.5$, whereas fit 7 allows y to be a free parameter. Both fits 6 and 7 give much better χ_v^2 values than fit 5 and still require large x values near 1. Fits with χ_v^2 comparable to fit 7 can be obtained with the condition $y < 0$ imposed (yielding $y=-0.075$) or by replacing $A_2^\pm \tau^{-y}$ with $A_2^\pm |\ln \tau|$. All such fits yield x close to 1 but give suspicious B and A_2^-/A_2^+ values. Indeed, examination of such fits shows that the fitting function is trying to mimic a step in B with $B^+ > B^-$. Thus we have also made fits with

$$C_p = A_1^\pm \tau^{-x} + A_2^\pm \tau^{-y} + A_3^\pm \tau^{-y'} + B^\pm + E(T - T_c). \quad (16b)$$

A justification for $B^+ \neq B^-$ can be based on the presence in Eq. (15) of terms of the form $\tau^{-x+2\Delta_1}$, which become τ independent (but not the same above and below T_c) if $x \approx 1$ and $\Delta_1 \approx 0.5$. Fits 2, 4, and 8 show that allowing $B^+ \neq B^-$ does not change the value of x , but fit 8 is significantly better than fit 5 for range C .

It is clear from fits 1–8 that $x \approx 1$ for the critical exponent of the leading singularity. A large value for the critical Sm-C–Sm-I exponent x is supported by fits made previously on C_p data for 8OSI. Although 8OSI is supercritical, one can exclude data for $\tau < 5 \times 10^{-4}$ (where ΔC_p is obviously rounded) and a pure power-law fit yields $x=0.80$ and $A^-/A^+=1.62$ [15].

Fits 9–12 are obtained with Eq. (16b) and the constraint $A_3^\pm \equiv 0$, which corresponds to the first corrections-to-scaling terms and a step in B that would arise from second corrections-to-scaling terms if $x \approx 1$. All four fits are quite good, even fit 12 in which x and y are both fixed, although the slope E has a small negative rather than the expected positive value. The 95%

confidence limits for x evaluated from the F test were determined by stepping x through a series of fixed values for fit 10 and the result is $x=1.06 \pm 0.08$. The quality of the representation of the data with fit 10 is shown in Fig. 7. It should be noted that the data taken at $\omega_0/9$ close to T_c may have uncertainties greater than $\pm 0.3\%$ of C_p due to the long acquisition time per point (~ 15 min). Note on the expanded temperature scale plot (upper curve) that the fit curves agrees well with several data points close to T_c that were excluded from the fit (i.e., the gap due to rounding could have been reduced to ~ 40 mK). The rounding of the C_p peak that is observed could be ascribed to either (a) a finite-frequency region where $C_p(\omega_0/9) < C_p(0)$ or (b) evidence that the 75% mixture is slightly supercritical. In view of the discussion of dynamics in Sec. III B and the narrow temperature range of this rounding, we feel that any deviation from the true critical composition will have only minor effect on the value of the critical exponent x .

Fits 13–15 represent fits with Eq. (16b) taking $A_3^\pm \neq 0$. In these fits one has $y' \equiv -0.5$, $A_3^\pm = -2.8 \pm 0.16$, and $A_3^-/A_3^+ = -0.010 \pm 0.0005$ for fit 13, where $y'=x-1.5$ with x being fixed at 1; $y'=x-1.5 = -0.443$, $A_3^\pm \approx 0.005 \pm 0.2$, and $A_3^-/A_3^+ \approx -378 \pm 18000$ for fit 14; and y' (free) $= -0.33 \pm 0.16$, $A_3^+ = 1.03 \pm 0.86$, and $A_3^-/A_3^+ = -1.3 \pm 1.6$ for fit 15. None of these fits has physically attractive parameters for the amplitudes of the $A_3^\pm \tau^{-y'}$ terms, but they confirm the stability of x to changes in the fitting function. An examination of $B_{\text{eff}}^\pm = A_3^\pm \tau^{-y'} + B^\pm + E\Delta T$ shows that these quantities are almost constant for fit 15 ($B_{\text{eff}}^+ = 2.247-2.287$ and $B_{\text{eff}}^- = 1.961-2.017$, but B_{eff}^+ varies by 10% for fit 13 and B_{eff}^- varies by 20% for fit 14).

In summary, all the good quality fits to range C (fits 7 and 9–15) are consistent with $x=1.06 \pm 0.08$. The most physically credible fits are 9–12, which explain deviations

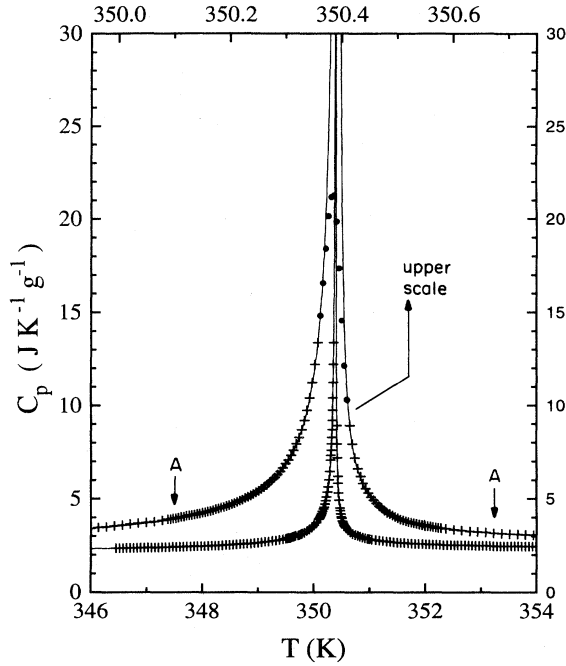


FIG. 7. Fit 10 with Eq. (16b) to the static heat capacity of the near-critical 75% mixture. The upper curve provides an expanded comparison of $C_p(\omega_0/9)$ data and fit 10 for temperatures near T_c (approximately range A , which is marked by arrows). The data points denoted by \bullet close to T_c are $C_p(\omega_0/9)$ points that were excluded from the fit. The lower curve corresponds approximately to range C (346.4–354.4 K). In order to improve the clarity of the display, only every third data point is plotted in the wings of the lower curve.

from the leading singularity $A_1^\pm \tau^{-x}$ with a single correction term (of comparable magnitude above and below T_c) and a step in B . The importance of these corrections to a simple power law is demonstrated in Fig. 8. This log-log plot of $[C_p - B^\pm - E(T - T_c)]$ versus τ would yield two parallel straight lines if a single-power form were adequate over the entire τ range. The quantity $[C_p - B - E(T - T_c)]$ is not sensitive to reasonable choices of E , but does of course depend on the choice of B , especially in the large- τ wings. The plot in Fig. 8 is based on the use of B and E values from fit 10. The crossover from $x \approx 1$ near T_c to a much smaller effective power at large τ is obvious.

One way to represent a strong crossover between two regimes is to use the Rudnick-Nelson form [24]

$$C_p = A^\pm \tau^{-\rho} (1 + a^\pm \tau^{-1/2})^\omega + B^\pm + E(T - T_c) \quad (17a)$$

$$= A_1^\pm \tau^{-x} \left[1 + \frac{1}{a^\pm} \tau^{1/2} \right]^\omega + B^\pm + E(T - T_c), \quad (17b)$$

where $x \equiv (\rho + 0.5\omega)$ and we have allowed for $B^+ \neq B^-$. In the limit where $a^\pm \tau^{-1/2} \ll 1$, this form yields Eq. (15) with $x = \rho$, $\Delta_1 = -0.5$, $D^\pm = \omega a^\pm$, etc. In the opposite limit where $a^\pm \tau^{-1/2} \gg 1$, one obtains Eq. (15) with $x = \rho + 0.5\omega$, $\Delta_1 = 0.5$, and $D^\pm = \omega/a^\pm$. The present data do not correspond to either of these asymptotic limits, but reasonable fits can be achieved with Eq. (17b). If

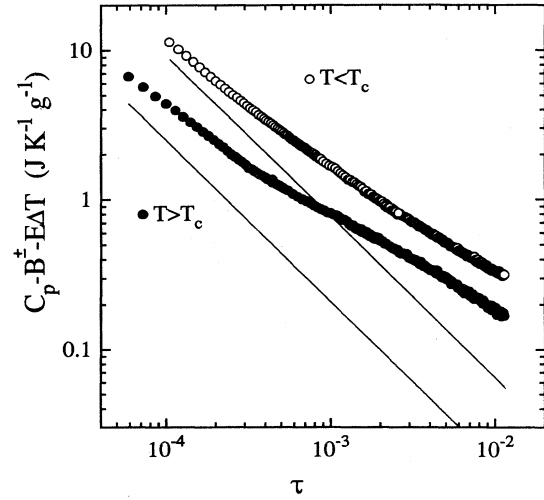


FIG. 8. log-log plot of critical heat capacity $[C_p - B^\pm - E(T - T_c)]$ versus the reduced temperature τ for a mixture with 75% 8OSI. Fit 10 values of $B^+ = 2.254$, $B^- = 2.048$, and $E = 0.0028$ are used and the leading singular terms $A_1^\pm \tau^{-x}$ given by fit 10 are represented by the straight lines. The solid lines both have slope $x = 1.075$.

$B^+ \equiv B^-$ is imposed, the parameters are $T_c = 350.397$ K, $B = 1.979$, $x = 1.139$, $\omega = 2 \pm 0.13$, $A_1^+ = 4.3 \times 10^{-5}$, $A_1^- / A_1^+ = 5.76$, $1/a^+ = 64.7 \pm 3$, $a^+ / a^- = (1/a^-) / (1/a^+) = 0.30$, and $E = 0.0039$ with $\chi^2 = 3.0$. When $B^+ \neq B^-$ is allowed, the parameters are $T_c = 350.392$ K, $B^+ = 2.38$, $\Delta B = 0.64$, $x = 1.091$, $\omega = 1.7 \pm 2.2$, $A_1^+ = 1.3 \times 10^{-4}$, $A_1^- / A_1^+ = 2.35$, $1/a^+ = 26 \pm 39$, $a^+ / a^- = 1.30$, and $E = -0.028$ with $\chi^2 = 1.2$. Again, we see that the exponent x lies near 1, but slightly larger.

Défontaines and Prost [13] show that the Sm-C–Sm-I critical point belongs to a new universality class that is the same as that for Sm-A–Sm-A critical points [25] and they give improved estimates for several critical exponents to first order in $\epsilon = 6 - d$, where d is the spatial dimension (3 in the present case). For the Sm-C–Sm-I transition, an attractive choice to describe changes in ordering is the smectic layer displacement u . If u is defined with respect to the critical layer thickness d_c , one finds that $C_6 - C_{6c} \propto \nabla_z u = (d - d_c) / d_c$, where $C_6 \propto |\psi|$ is the intensity of the sixfold x-ray scattering pattern in a hexatic material [13]. The quantity $M_z = \langle \nabla_z u \rangle$ is the analog of $\langle \rho - \rho_c \rangle$ in the case of liquid-vapor critical phenomena. The critical heat capacity at zero strain is given in terms of the theoretical thermal scaling field \tilde{t} by

$$\Delta C_p(M_z = 0) = \Delta C_p(d = d_c) \propto \tilde{t}^{-\alpha}, \quad (18)$$

but this quantity is not experimentally accessible from measurements made at constant composition and constant pressure.

The singular part of the zero-stress critical heat capacity along a constant pressure path has the following scaling form [25,26]:

$$\Delta C_p(h, \tilde{t}) = \lambda^{\gamma/\nu_1} f(\lambda^{1/\nu_1} \tilde{t}, \lambda^{\Delta/\nu_1} h), \quad (19)$$

where h is the scaling field conjugate to the layer

compression $\nabla_z u$, the critical exponent $\Delta = \beta + \gamma$, and ν_1 is the in-plane smectic correlation critical exponent. The theoretical fields $\tilde{\tau}$ and h are related to the physical variables τ and $\Delta\mu^{\text{crit}}$ (chemical potential difference) in a material at the critical composition by

$$h = a\tau + b\Delta\mu^{\text{crit}}, \quad (20a)$$

$$\tilde{\tau} = c\tau + d\Delta\mu^{\text{crit}}. \quad (20b)$$

If the terms involving $\Delta\mu^{\text{crit}}$ can be neglected in Eqs. (20), the critical path is a straight line in the $(h, \tilde{\tau})$ plane and one has two limiting regimes for the experimental zero-stress heat capacity [13,26]

$$\Delta C_p(T) \propto |h|^{-\gamma/\Delta} \propto \tau^{-\gamma/\Delta} \quad \text{for } |h| \gg |\tilde{\tau}|^\Delta \text{ (region 1)}, \quad (21a)$$

$$\Delta C_p(T) \propto |\tilde{\tau}|^{-\gamma} \propto \tau^{-\gamma} \quad \text{for } |h| \ll |\tilde{\tau}|^\Delta \text{ (region 2)}, \quad (21b)$$

where γ is the susceptibility exponent, β is the order parameter exponent, and $\Delta = \beta + \gamma$. The crossover region, where $|h| \simeq |\tilde{\tau}|^\Delta$, has a finite width that depends on the specific form of the scaling function $f(\tilde{\tau}, h)$. Since one generally expects $\Delta > 1$, the crossover region lies close to the $\tilde{\tau}$ axis near the critical point and the asymptotic behavior close to T_c will correspond to region 1 unless h is quite small along the experimental path. If the terms involving $\Delta\mu^{\text{crit}}$ are not negligible in Eqs. (20), the critical path is curved close to the critical point [$|h| \sim \tau^{\Delta/(1-\alpha)}$] and Fisher renormalization will occur, yielding

$$\Delta C_p(T) \propto \tau^{-\gamma/(1-\alpha)} \quad (21c)$$

as the asymptotic form in both region 1 and 2 [26].

There are three possibilities for the experimental exponent $x = 1.06 \pm 0.08$: (a) $x = \gamma/\Delta$, (b) $x = \gamma$, and (c) $x = \gamma/(1-\alpha)$. The theoretical estimate of γ/Δ for the new universality class is $0.47 < \gamma/\Delta < 0.54$ [13] and the best experimental value is 0.45 ± 0.08 [26], whereas $\gamma/\Delta = 0.67$ (mean field) and $\gamma/\Delta = 0.79$ (3D XY and 3D Ising). Thus $x = \gamma/\Delta$ is eliminated as a possibility for any of these universal classes. If the path is in region 2 and the new universality class governs the exponent values, one obtains $\gamma = x \simeq 1$, $\beta \simeq \gamma \simeq 1$ (since $\gamma/\Delta \simeq \frac{1}{2}$ and $\Delta \equiv \beta + \gamma$), $\alpha \simeq -1$, and $\nu \simeq 1$ (due to the scaling equalities $\alpha + 2\beta + \gamma = 2$ and $2 - \alpha = 3\nu$). If the path is dominated by Fischer renormalization and the new universality class is pertinent, then $\gamma/(1-\alpha) = x \simeq 1$ and $\alpha \simeq \frac{1}{2}$, $\beta \simeq \gamma \simeq \frac{1}{2}$, and $\nu \simeq \frac{1}{2}$.

The decision about which of the limiting paths is the proper assignment for measurements at constant $X = X_c$ for a Sm-C-Sm-I system can be greatly assisted by consideration of the variation in the smectic layer thickness $d(T)$ obtained from x-ray data:

$$d(T) = d_c + a^\pm \tau^\nu + e(T - T_c), \quad (22)$$

where d_c is the layer spacing at the critical point and the amplitudes a^\pm have opposite signs [26]. The critical exponent is $z = 1/\delta \equiv \beta/\Delta$ for region 1, $z = \beta$ for region 2,

and $z = \beta/(1-\alpha)$ if Fisher renormalization occurs. X-ray studies have not been made on a 8SI plus 8OSI mixture with $X = 75$, but do exist for a closely related Sm-C-Sm-I critical mixture TB10A + (10)OSI [27]. The experimental value of the exponent z in that system is $z = 0.55 \pm 0.06$. This result confirms our rejection of region 1 since for that path $x = \gamma/\Delta$ and $z = \beta/\Delta$, which requires that $x + z = 1$, whereas experimental x and z sum to 1.61 ± 0.14 .

Thus we need to review the possibility of a path in region 2 or a Fisher renormalized path. Neither of these paths is consistent with critical behavior governed by the new universality class since $\gamma/\Delta \simeq 0.5$ requires $\beta \simeq \gamma$ and therefore $x \simeq z$, whereas experimentally $x \simeq 2z$. The data are, however, consistent with a path in region 2 with mean-field values of the critical exponents: $\alpha = 0$, $\beta = \frac{1}{2}$, $\gamma = 1$, and $\Delta = 1.5$. Furthermore, the scaling field h in a Sm-C-Sm-I system is like a uniaxial stress conjugate to the smectic layer thickness [since $(d - d_c)/d_c \propto C_6 - C_{6c}$] and it seems reasonable that such a stress axis would be roughly normal to the $T-X$ plane. This leads to the path lying in region 2. Therefore, we conclude that $x = \gamma = 1.06 \pm 0.08$ and $z = \beta = 0.55 \pm 0.06$. If one disregards the x-ray information on layer thickness $d(T)$, then the Sm-Sm universality class could dominate the critical behavior, but one cannot decide on the basis of C_p data alone whether the path is in region 2 or is Fisher normalized.

It may seem strange to claim mean-field ΔC_p behavior when Fig. 4 clearly shows a roughly symmetrical curve with excess heat capacity above T_c as well as below. However, one must keep in mind that $\Delta C_p(X_c, T)$ along a path in region 2 is really a thermal probe of a susceptibility-like quantity that is governed by the critical exponent γ . Recall that C_p for a simple fluid near its liquid-gas critical point varies like $\tau^{-\gamma}$. Thus Fig. 4 shows a Curie-Weiss divergence (modified by correction-to-scaling terms). However, it should be noted that in this Sm-C-Sm-I situation one does not have the amplitude ratio expected from Landau mean-field theory for the susceptibility χ since $\chi^-/\chi^+ \leq 0.5$ whereas our $A_1^-/A_1^+ > 2$. This suggests inverted mean-field behavior, which will be discussed at the end of this section.

An essential question, is why does the behavior near a Sm-C-Sm-I critical point exhibit mean-field character instead of the new universality behavior predicted by theory and seen near the related Sm- A_d -Sm- A_2 critical point? It seems likely that the explanation can be provided by the Ginzburg criterion for predicting the width τ_{crit} of the critical regime [28]. For $\tau < \tau_{\text{crit}}$, the system is dominated by critical fluctuation behavior. For $\tau > \tau_{\text{crit}}$, mean-field behavior occurs. Since $\tau_{\text{crit}} \propto (\xi_0)^{-6}$, where ξ_0 is the bare correlation length, the size of the critical region is very sensitive to the range of correlations in each particular case. For example, both N-Sm- A and Sm- A -Sm-C transitions belongs to the 3D XY universality class: N-Sm- A systems exhibit critical behavior since ξ_0 is small (typically $\xi_{10} \simeq 1.5 \text{ \AA}$, $\xi_{10} \simeq 5 \text{ \AA}$), whereas Sm- A -Sm-C systems are mean field since ξ_0 is large (typically $\xi_0 \simeq 20 \text{ \AA}$) [29,30]. We propose that (a) ξ_0 is small for

Sm- A_d -Sm- A_2 critical systems, which implies a broad critical reduced temperature regime and critical values of the exponents, as observed [26], and (b) ξ_0 is large for Sm-C-Sm-I critical systems, which would result in a very small τ_{crit} and the mean-field exponents. Although high-resolution x-ray data do not yet exist to confirm this proposal, it seems reasonable in view of the fact that BO order and tilt order are coupled in Sm-C-Sm-I systems and tilt ordering is well established above T_c , which is ~ 40 K below the Sm-A-Sm-C transition temperature for the $X_c=75$ critical sample. There is, however, another possible explanation for mean-field behavior near this Sm-C-Sm-I critical point. It has been shown [25] that the upper critical dimension for this new universality class drops to 2.5 when splay-type critical fluctuations are suppressed by either a magnetic field or a local strain field. Thus mean-field behavior might arise in poly-domain samples due to significant residual strains.

In spite of the fact that the Sm-C-Sm-I critical point occurs deep in the Sm-C phase, the tilt angle θ is not saturated and temperature independent. The value of $\langle \theta \rangle$ in the Sm-C phase of 8OSI films increases over a range of ~ 3.5 K on cooling toward the Sm-C-Sm-I transition and then levels off at an essentially constant value for temperatures in the Sm-I phase [18]. This means that the “tilt field” $H \sim |\theta|^6$ is not constant for $T > T_c$, and this could have a significant effect since the $H\Psi = (h_6 + h_{12})|\theta|^6\Psi$ term plays an important role. Indeed, the deviations between our C_p data and fitting equations (16) and (17) are small and random for $T < T_c$, but are somewhat larger and show systematic trends for $T > T_c$. One needs an analytic form for fitting data along a path where the tilt field H varies as a function of reduced temperature τ . Since the tilt angle $\langle \theta \rangle$ has a roughly inverted Landau shape (varies above T_c and is approximately constant below T_c), that may explain our “inverted” amplitude ratio A_1^- / A_1^+ .

The implication of the above discussion is that there are significant contributions to C_p that are due to Ψ - θ coupling. Fluctuations in the bond-orientational order parameter Ψ can drive fluctuations in θ and these contribute to C_p (somewhat analogously to the coupling between the smectic- A order parameter ψ and the orientational order S near the N -Sm- A transition). Since $\langle \theta \rangle$ is connected with the layer thickness d and the Défontaines-Prost theory [13] uses $\nabla_z u = (d - d_c) / d_c$ as the BO order parameter, this would seem an attractive starting point. Note, however, the harmonics of Ψ play an important role in the x-ray study of tilted hexatic order [9,14] and there is a difficulty in dealing with harmonics of Ψ in a theory that makes Ψ a scalar.

B. Dynamic behavior near T_c

The heat capacity is traditionally considered to be a static thermodynamic quantity and the values of C_p extracted from ac calorimetry at $\omega_0=0.196$ (temperature oscillation frequency 31.25 mHz) are almost always the static values $C_p(0)$. However, recent frequency-dependent measurements on glasses [31,32] have shown that C_p can

be thought of as a dynamical response function like the susceptibility. If a system contains slow degrees of freedom that relax with a characteristic time constant τ_R , then this will be reflected in the specific heat. In the frequency domain, $C_p^*(\omega)$ will be a complex quantity whose real part shows dispersion and whose imaginary part exhibits a peak at frequencies near $\omega = \tau_R^{-1}$. In formal terms, $C_p^*(\omega)$ can be defined by

$$C_p^*(\omega) = C_p(0) + \frac{i\omega}{k_B T^2 \rho V} \int_0^\infty dt e^{i\omega t} \langle \delta H(0) \delta H(t) \rangle, \quad (23)$$

where $C_p(0)$ is the usual static specific heat and $\langle \delta H(0) \delta H(t) \rangle$ is the time-dependent correlation function for the total enthalpy where enthalpy fluctuations are given by $\delta H(t) = H(t) - \langle H \rangle$. Thus the measurement of $C_p(\omega)$ probes the enthalpy relaxation that is governed by the slow dynamics of the system.

Unlike the case of glasses, we are concerned here with critical dynamics—the critical slowing down of cooperative ordering phenomena. The theoretical prediction for order-parameter relaxation is $\tau_R \sim \xi^z \sim \tau^{-z\nu}$, where τ is the reduced temperature [33]; this has been confirmed in mean-field and critical universality systems. The value of $z\nu$ is 1 for conventional van Hove critical slowing down and is greater than 1 for various dynamic universality classes when critical fluctuations play a dominant role [33]. Thus one expects dispersion, a frequency dependence of $\text{Re}C_p(\omega)$, and peak values for $\text{Im}C_p(\omega)$ to occur very close to T_c for our sample with $X \simeq X_c$ if $\omega\tau_R$ becomes large (say > 0.1) for our experimental ω range. This behavior is demonstrated by Figs. 5 and 6, where $|C_p^*(\omega)| = C_{p,B}$ is shown in Fig. 5 instead of $\text{Re}C_p(\omega)$, but the dispersion is clear.

In general we expect

$$C_p^*(\omega) = C_p(\infty) + \Delta C_p(\infty) G(\omega\tau_R) - i \Delta C_p(\infty) \omega\tau_R \times F(\omega\tau_R), \quad (24)$$

where $\Delta C_p(\infty) \equiv C_p(0) - C_p(\infty)$. $F(\omega\tau_R)$ and $G(\omega\tau_R)$ are relaxation functions with limiting behavior for fluctuation-dominated systems given by

$$F(\omega\tau_R) = G(\omega\tau_R) = 1 \quad \text{if } \omega\tau_R \ll 1, \quad (25a)$$

$$F(\omega\tau_R) \propto (\omega\tau_R)^{-(1+x/z\nu)} \quad \text{if } \omega\tau_R \gg 1, \quad (25b)$$

$$G(\omega\tau_R) \propto (\omega\tau_R)^{-x/z\nu} \quad \text{if } \omega\tau_R \gg 1, \quad (25c)$$

where x is the static critical exponent for ΔC_p . See Refs. [34,35] for further details about the form of dynamic scaling functions. If there is a single Debye relaxation process, one has

$$F(\omega\tau_R) = G(\omega\tau_R) = 1 / (1 + \omega^2 \tau_R^2) \quad \text{for all } \omega\tau_R. \quad (26)$$

It is convenient to analyze dynamic response data by making Cole-Cole plots of $\text{Im}C_p(\omega)$ versus $\text{Re}C_p(\omega)$, as is done for the dielectric response in ferroelectric solids and liquid crystals [36]. Such plots require interpolations of $\text{Re}C_p(\omega)$ and $\text{Im}C_p(\omega)$ data values at a set of fixed temperatures. We have done this at 10-mK intervals over

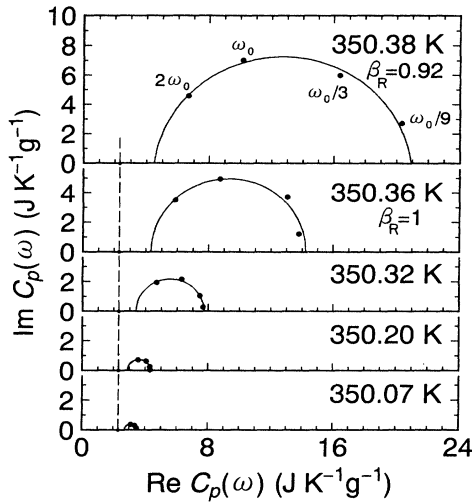


FIG. 9. Cole-Cole plots of the real and the imaginary parts of the heat capacity near $T_c \approx 350.393$ K. The dashed line represents the variation of $C_{p,B}$ with temperature.

the range 349.98–350.71 K to obtain 74 “data sets,” and typical Cole-Cole plots are given in Fig. 9 for five temperatures below T_c . When the relaxation has the Debye form, this display corresponds to a semicircle with $C_p(0)$ being the large intercept on the real axis and $C_p(\infty)$ being the small intercept. Deviations from the Debye form were observed only for the five temperatures $T=350.37$, 350.38, 350.39, 350.40, and 350.41 K. In these cases one can use the empirical form $C_p(\omega) = C_p(\infty) + \Delta C_p(\infty) / [1 + (i\omega\tau_R)^{\beta_R}]$. The adjustable β_R fitting values, which were found to $\beta_R = 0.949, 0.921, 0.916, 0.946, \text{ and } 0.981$, respectively, do not represent very significant deviations from Debye ($\beta_R = 1$) behavior. Note that $C_p(\infty)$ does not equal $C_{p,B}$, a feature that we will return to later.

The relaxation times τ_R obtained from Cole-Cole fits are shown in Fig. 10 and the $C_p(0)$ and the $C_p(\infty)$ tem-

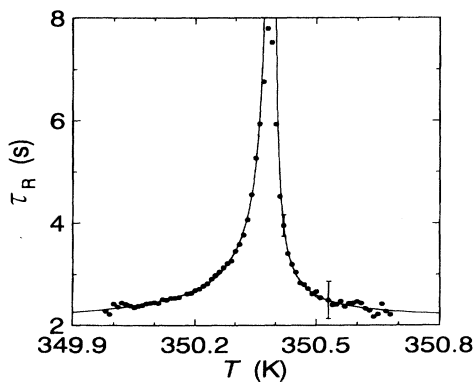


FIG. 10. Relaxation time τ_R associated with the Sm-C-Sm-I critical point in the 8SI plus 8OSI mixture with $X=75$. Two typical error bars are shown to indicate the uncertainties in extracting τ_R values from our ac heat capacity data. The smooth curve represents a fit with Eq. (27a) using parameter values given in the text.

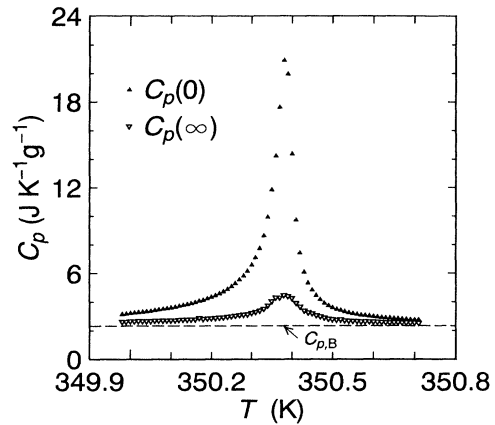


FIG. 11. Temperature dependence of $C_p(0)$ and $C_p(\infty)$ extracted from the present ac $C_p(\omega)$ data using Eqs. (24) and (26). The variation of $C_{p,B} = 2.34 + 0.0062(T - T_c)$ is also shown.

perature dependences are given in Fig. 11. The behavior of τ_R as a function of $(T - T_c)$ can be examined in two ways: (i) fit τ_R with a power-law form $\tau_0^\pm (T - T_c)^{-z\nu}$ and determine $z\nu$ or (ii) plot τ_R vs $C_p(0)$ as shown in Fig. 12. The power-law form provides a good fit if one allows for a temperature-independent term k^\pm ,

$$\tau_R = k^\pm + \tau_0^\pm (T - T_c)^{-z\nu}. \quad (27a)$$

The available fitting range is from -1.2×10^{-3} to $+0.8 \times 10^{-3}$ in reduced temperature (roughly range A for C_p) and the fitting parameters are $k^+ = 2.095$ s, $k^- = 1.965$ s, $\tau_0^+ = (6.08 \pm 2.17) \times 10^{-2}$, $\tau_0^- / \tau_0^+ = 2.53 \pm 0.50$, and $z\nu = 0.95 \pm 0.07$ with $\chi^2_\nu = 1.20$. Note that the value $z\nu = 0.95$ is very close to the expected van Hove value $z\nu = 1$. The plot given in Fig. 12 makes it clear that τ_R is also well described by the empirical form

$$\tau_R = k^\pm + l C_p(0), \quad (27b)$$

where $\chi^2_\nu = 1.85$ for a fit with $k^+ = 1.455$ s above T_c , $k^- = 1.345$ s below T_c , and the coefficient $l = 0.314$ has the same value above and below T_c .

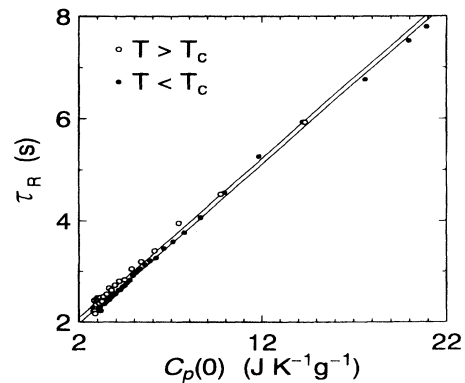


FIG. 12. Plot of τ_R versus the static heat capacity $C_p(0)$ for the 8SI plus 8OSI mixture with $X=75$. The lines represent a fit with Eq. (27b) using parameter values given in the text.

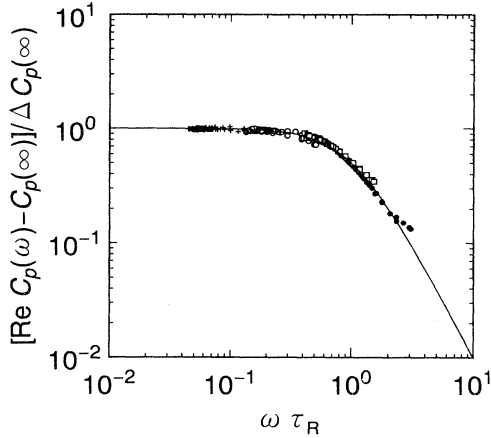


FIG. 13. Dynamic scaling plot of $[\text{Re}C_p(\omega) - C_p(\infty)] / \Delta C_p(\infty)$ versus $\omega\tau_R$. The solid line is the Debye scaling function $G(\omega\tau_R)$ with an asymptotic ($\omega\tau_R \gg 1$) slope of -2 . Data both above and below T_c are included. The symbols have the same meanings as in Figs. 5 and 6.

A dynamic scaling representation of our $C_p(\omega)$ data is given in Figs. 13 and 14, where $[\text{Re}C_p(\omega) - C_p(\infty)] / \Delta C_p(\infty)$ and $\text{Im}C_p(\omega) / \Delta C_p(\infty) \omega\tau_R$ are plotted versus $\omega\tau_R$. The values of $\Delta C_p(\infty)$ and τ_R were obtained from Cole-Cole plots with $\beta_R = 1$. Figures 13 and 14 show excellent data collapse and the experimental points conform quite closely to the Debye form of $F(\omega\tau_R)$ and $G(\omega\tau_R)$, as expected from the Cole-Cole plots.

The last issue is the discrepancy between $C_p(\infty, T)$, and $C_{p,B}(T)$ shown in Figs. 9 and 11. It is possible that this indicates the presence of two relaxation processes: a very slow process with relaxation time τ_R greater than 2 s (frequency $f_{R1} < 0.5$ Hz), which we have characterized with $C_p(\omega)$ data taken over the frequency range 0.0035 Hz $< f_{ac} < 0.06$ Hz, and a faster process with relaxation times $\tau_2 < \sim 0.05$ s (f_{R2} value > 20 Hz). Since our

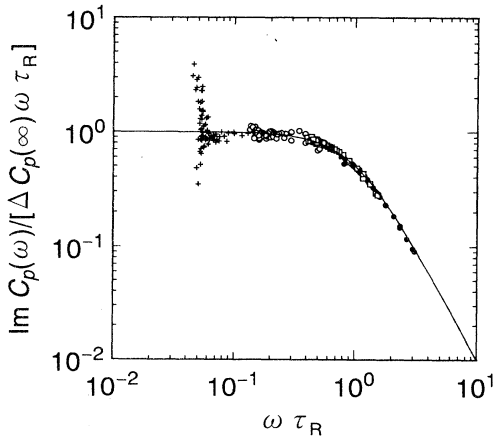


FIG. 14. Dynamic scaling plot of $\text{Im}C_p(\omega) / \Delta C_p(\infty) \omega\tau_R$ versus $\omega\tau_R$. The solid line is the Debye scaling function $F(\omega\tau_R)$. Data both above and below T_c obtained at $\omega_0/9$ (+) show considerable scatter since the numerator and the denominator are very small and thus less precise at this low frequency.

highest frequency is $2\omega_0 = 0.392$, the maximum value of $\omega\tau_2$ would be only 0.02 and such a second relaxation with a small relaxation strength $[C_p(\infty) - C_{p,B}]$ would have no effect on the data reported here. In the case of dielectric relaxation near the Sm-A–Sm-C* transition, there are two distinct relaxation modes—the soft mode (amplitude of tilt order parameter) and the Goldstone mode (phase of tilt order parameter) [36]. Because the phase (azimuthal angle) of the tilt order parameter in Sm-C* can be reoriented by a perturbing external electric field, this Goldstone contribution extends over the entire range of the Sm-C* phase. In our case, there is coupled BO order and tilt order which evolve critically as $T \rightarrow T_c$ along the path $X = X_c$. This coupled order parameter has an amplitude and phase and both can show critical slowing down at T_c . Thus we propose to extend the frequency range of our ac calorimeter in order to search for a possible second critical relaxation process.

IV. SUMMARY

A new calorimeter design capable of operation in an ac mode and in a nonadiabatic scanning mode has been used to provide the first high-resolution study of a Sm-C–Sm-I critical point. Although predicted to belong to the new universality class that includes Sm-A_d–Sm-A₂ and Sm-C*–Sm-C* critical points, the static C_p data for a 8SI plus 8OSI critical mixture exhibit a somewhat complicated mean-field behavior in which the leading singularity varies like $|T - T_c|^{-x}$ with $x = \gamma = 1.06 \pm 0.08$.

It is proposed that mean-field rather than fluctuation behavior is observed due to long bare correlation lengths that lead to an inaccessibly small critical region (Ginzburg criterion). There are also indications that the C_p data are influenced by strong tilt–bond-orientational coupling $H\Psi = (h_6 + h_{12})|\theta|^6\Psi$, where the tilt field H varies as a function of temperature for $T > T_c$. Additional theoretical work is needed on the effects of θ - Ψ coupling.

The improved stability of measurements of $\tan\phi$, where $\phi - (\pi/2)$ is the phase shift between $T_{ac}(t)$ and the input power $P_{ac}(t)$, allows us to characterize the real and the imaginary parts of a complex frequency-dependent heat capacity $C_p^*(\omega)$. Dispersion [i.e., frequency dependence of $\text{Re}C_p(\omega)$] and nonzero $\text{Im}C_p(\omega)$ data were obtained over the range $f_{ac} = 3.5$ –62.5 mHz or $\omega = \omega_0/9$ – $2\omega_0$, where our standard operating frequency for ac calorimetry is $\omega_0 = 0.196$. Dynamic data obtained over the range $\omega\tau = 0.045$ –3 conform to a single Debye relaxation and the critical relaxation time τ_R exhibits classical critical behavior with τ_R diverging like the static heat capacity $C_p(\omega=0)$, i.e., $z\nu \simeq 1$.

ACKNOWLEDGMENTS

The authors wish to thank J. Prost, A. Aharony, I. Oppenheim, and Z. Kutnjak for helpful and stimulating discussions. This work was supported in part by National Science Foundation Grant No. DMR93-11853. One of the authors (H. Y.) thanks Professor K. Ema for support during his stay at MIT.

- [1] R. Pindak, D. E. Moncton, S. C. Davey, and J. W. Goodby, *Phys. Rev. Lett.* **46**, 1135 (1981).
- [2] C. C. Huang, J. M. Viner, R. Pindak, and J. W. Goodby, *Phys. Rev. Lett.* **46**, 1289 (1981).
- [3] T. Pitchford, G. Nounesis, S. Dumrongrattana, J. M. Viner, and C. C. Huang, *Phys. Rev. A* **32**, 1938 (1985).
- [4] C. C. Huang, G. Nounesis, and D. Guillon, *Phys. Rev. A* **33**, 2602 (1986).
- [5] C. C. Huang, G. Nounesis, R. Geer, J. W. Goodby, and D. Guillon, *Phys. Rev. A* **39**, 3741 (1989).
- [6] G. Nounesis, R. Geer, H. Y. Liu, C. C. Huang, and J. W. Goodby, *Phys. Rev.* **40**, 5468 (1989).
- [7] T. Stoebe, C. C. Huang, and J. W. Goodby, *Phys. Rev. Lett.* **68**, 2944 (1992).
- [8] R. Bruinsma and G. Aeppli, *Phys. Rev. Lett.* **48**, 1625 (1982).
- [9] A. Aharony, R. J. Birgeneau, J. D. Brock, and J. D. Litster, *Phys. Rev. Lett.* **57**, 1012 (1986).
- [10] J. V. Selinger, *J. Phys. (Paris)* **49**, 1387 (1988).
- [11] I. M. Jiang, S. N. Huang, J. Y. Ko, T. Stoebe, A. J. Jin, and C. C. Huang, *Phys. Rev. B* **48**, R3240 (1993).
- [12] D. R. Nelson and B. I. Halperin, *Phys. Rev. B* **21**, 5312 (1980); R. Bruinsma and D. R. Nelson, *ibid.* **23**, 402 (1981).
- [13] A. D. Défontaines and J. Prost, *Phys. Rev. E* **47**, 1184 (1993).
- [14] J. D. Brock, A. Aharony, R. J. Birgeneau, K. W. Evans-Lutterodt, J. D. Litster, P. M. Horn, G. B. Stephenson, and A. R. Tajbakhsh, *Phys. Rev. Lett.* **57**, 98 (1986); J. D. Brock, D. Y. Noh, B. R. McClain, J. D. Litster, R. J. Birgeneau, A. Aharony, P. M. Horn, and J. C. Liang, *Z. Phys. B* **74**, 197 (1989).
- [15] C. W. Garland, J. D. Litster, and K. J. Stine, *Mol. Cryst. Liq. Cryst.* **170**, 71 (1989).
- [16] D. Y. Noh, J. D. Brock, J. D. Litster, R. J. Birgeneau, and J. W. Goodby, *Phys. Rev. B* **40**, 4920 (1989).
- [17] K. J. Stine and C. W. Garland, *Mol. Cryst. Liq. Cryst.* **188**, 91 (1990).
- [18] S. Sprunt, M. S. Spector, and J. D. Litster, *Phys. Rev. A* **45**, 7355 (1992); M. S. Spector, Ph.D. thesis, Massachusetts Institute of Technology, 1992.
- [19] J. Budai, R. Pindak, S. C. Davey, and J. W. Goodby, *J. Phys. Lett.* **45**, L1053 (1984).
- [20] J. W. Goodby and G. W. Gray, *J. Phys. (Paris) Colloq.* **40**, C3-27 (1979); A. J. Leadbetter, J. P. Gaughan, B. Kelly, G. W. Gray, and J. Goodby, *ibid.* **40**, C3-178 (1979).
- [21] J. Przedmojski, R. Dabrowski, B. Pura, K. Zickert, and S. Gierlotka, *Mol. Cryst. Liq. Cryst.* **151**, 171 (1987).
- [22] C. W. Garland, *Thermochim. Acta* **88**, 127 (1985).
- [23] K. Ema, T. Uematsu, A. Sugata, and H. Yao, *Jpn. J. Appl. Phys.* **32**, 1846 (1993), and references cited therein; H. Yao, H. Nagano, Y. Kawase, and K. Ema, *Biochem. Biophys. Acta* **1212**, 73 (1994).
- [24] J. Rudnick and D. R. Nelson, *Phys. Rev. B* **13**, 2208 (1976).
- [25] Y. Park, T. C. Lubensky, P. Barois, and J. Prost, *Phys. Rev. A* **37**, 2197 (1988); Y. Park, T. C. Lubensky, and J. Prost, *Liq. Cryst.* **4**, 435 (1989).
- [26] X. Wen, C. W. Garland, R. Shashidhar, and P. Barois, *Phys. Rev. B* **45**, 5131 (1992).
- [27] S. Krishna Prasad, D. S. Shankar Rao, S. Chandrasekhar, M. E. Neubert, and J. W. Goodby, *Phys. Rev. Lett.* **74**, 270 (1995).
- [28] V. L. Ginzburg, *Fiz. Tverd. Tela* **2**, 2031 (1960) [*Sov. Phys. Solid State* **2**, 1824 (1961)].
- [29] R. J. Birgeneau, C. W. Garland, G. B. Kasting, and B. M. Ocko, *Phys. Rev. A* **24**, 2624 (1981).
- [30] R. J. Birgeneau, C. W. Garland, A. R. Kortan, J. D. Litster, M. Meichle, and B. M. Ocko, *Phys. Rev. A* **27**, 1251 (1983).
- [31] N. O. Birge, *Phys. Rev. B* **34**, 1631 (1986); N. O. Birge and S. R. Nagel, *Rev. Sci. Instrum.* **58**, 1464 (1987).
- [32] D. H. Jung, T. W. Kwon, D. J. Bae, I. K. Moon, and Y. H. Jeong, *Meas. Sci. Tech.* **3**, 475 (1992).
- [33] P. C. Hohenberg and B. I. Halperin, *Rev. Mod. Phys.* **49**, 435 (1977), and references cited therein.
- [34] J. Hu, J. O. Fossum, C. W. Garland, and P. W. Wallace, *Phys. Rev. B* **33**, 6331 (1986).
- [35] V. Dohm (private communication).
- [36] A. Levstik, T. Carlsson, C. Filipic, I. Levstik, and B. Zeks, *Phys. Rev. A* **35**, 3527 (1987); C. Filipic, T. Carlsson, A. Levstik, B. Zeks, R. Blinc, F. Gouda, S. T. Lagerwall, and K. Skarp, *ibid.* **38**, 5833 (1988).